Geophysical Journal International

Geophys. J. Int. (2013) **192,** 666–670 doi: 10.1093/gji/ggs052

EXPRESS LETTER

Interferometric redatuming by sparse inversion

Joost van der Neut[1] and Felix J. Herrmann[2]

[1]*Department of Geoscience and Engineering, Delft University of Technology, PO Box* 5048, 2600 *GA Delft, the Netherlands.*
E-mail: j.r.vanderneut@tudelft.nl
[2]*Department of Earth, Ocean and Atmospheric Sciences, University of British Columbia,* 2357 *Main Mall, Vancouver, BC* V6T 1Z4, *Canada*

Accepted 2012 October 31. Received 2012 October 31; in original form 2012 September 11

SUMMARY

Assuming that transmission responses are known between the surface and a particular depth level in the subsurface, seismic sources can be effectively mapped to this level by a process called interferometric redatuming. After redatuming, the obtained wavefields can be used for imaging below this particular depth level. Interferometric redatuming consists of two steps, namely (i) the decomposition of the observed wavefields into downgoing and upgoing constituents and (ii) a multidimensional deconvolution of the upgoing constituents with the downgoing constituents. While this method works in theory, sensitivity to noise and artefacts due to incomplete acquisition require a different formulation. In this letter, we demonstrate the benefits of formulating the two steps that undergird interferometric redatuming in terms of a transform-domain sparsity-promoting program. By exploiting compressibility of seismic wavefields in the curvelet domain, the method not only becomes robust with respect to noise but we are also able to remove certain artefacts while preserving the frequency content. Although we observe improvements when we promote sparsity in the redatumed data space, we expect better results when interferometric redatuming would be combined or integrated with least-squares migration with sparsity promotion in the image space.

Key words: Inverse theory; Interferometry; Controlled source seismology.

1 INTRODUCTION

Seismic reflection imaging of the subsurface relies on detailed and often difficult to obtain information on the background-velocity model. To overcome this difficulty, various interferometric methods have recently been introduced that are velocity-independent (Schuster & Zhou 2006). Opposed to conventional reflection imaging, these new imaging methods require the transmission responses from sources at the surface to receivers in the subsurface just above the target zone. These receivers can be physically deployed, as in the virtual-source method of Bakulin & Calvert (2006), or they can be estimated from surface data, using a new methodology developed by Broggini *et al.* (2012) and Wapenaar *et al.* (2012a,b).

Interferometric redatuming is the process of transforming the recorded or estimated transmission data into virtual reflection data as if sources and receivers are located in the subsurface just above the target zone. In principle, this redatuming can be done by decomposing the transmitted wavefields into downgoing and upgoing constituents, followed by multidimensional deconvolution of the upgoing constituents with the downgoing constituents (Schuster & Zhou 2006; Wapenaar *et al.* 2008). As such, interferometric redatuming is related to the focal transform (Berkhout & Verschuur 2006), where a full wavefield is deconvolved with another full wavefield.

Unfortunately, carrying out multidimensional deconvolutions in practice is challenging because of the effects of finite bandwidth/aperture and source–receiver array directivity that hamper observed seismic wavefields. The effects lead to small singular values, which in turn lead to instabilities during the inversion. To overcome this problem of small singular values, which makes the interferometric redatuming problem poorly conditioned, regularization is required to constrain the solution (Minato *et al.* 2011; van der Neut 2012). Typically, this regularization comes in the form of an additional functional that penalizes the energy of the solution. While often effective, this sort of regularization can lead to an undesired loss in resolution. Regularizations based on curvelet-domain sparsity promotion, on the other hand, are designed to preserve resolution by taking advantage of the property that seismic wavefields are compressible in the curvelet domain (Herrmann *et al.* 2008). Curvelets exhibit this property because they behave, by virtue of their multiscale, multidirectional, and parabolic scaling properties, as localized eigenfunctions of high-frequency solution operators of the wave equation (Candès *et al.* 2006a). This property, which allows curvelets to detect wave front sets, explains their successful application to problems involving field data that range from missing-trace interpolation (Herrmann & Hennenfent 2008) to the recovery of simultaneously acquired marine data (Mansour *et al.* 2012) and the estimation of primaries by sparse inversion (Lin & Herrmann 2011).

Motivated by the successful applications of this transform, we apply this type of regularization to the interferometric redatuming problem. Our letter is organized in three steps: (i) decomposition of the transmitted wavefields into downgoing and upgoing constituents; (ii) redatuming of the source wavefield towards the receiver level and (iii) creation of the subsurface image from the redatumed data. Each step can be interpreted as a separate inverse problem that can benefit from sparsity promotion in the curvelet domain.

2 WAVEFIELD DECOMPOSITION

By deploying downhole geophones and hydrophones along a horizontal borehole, we record the vertical particle-velocity field $\mathbf{v}$ and the pressure field $\mathbf{p}$ induced by monopole sources at the surface (Mehta *et al.* 2010). After discretization, these fields are expressed as vectors that depend on time, the horizontal position in the borehole, and the source location. Under certain conditions, we can also estimate these transmission responses directly from surface data (Wapenaar *et al.* 2012b). Before redatuming of the sources, we need to decompose the observed pressure and particle-velocity wavefields into their downgoing, denoted by $\mathbf{d}$, and upgoing, denoted by $\mathbf{u}$, components. Following Claerbout (1971), we relate these time-domain one-way wavefield constituents to the recorded pressure and particle velocity by the following composition relation:

$$\begin{bmatrix} \mathbf{p} \\ \mathbf{v} \end{bmatrix} = \mathbf{L} \begin{bmatrix} \mathbf{d} \\ \mathbf{u} \end{bmatrix}. \tag{1}$$

In this expression, the symbol $\mathbf{L}$ stands for the wavefield composition matrix that involves Fourier transformation, followed by application of pseudo-differential operators that compose the time-harmonic wavefield from its downgoing and upgoing constituents, and inverse Fourier transformation. The wavefield composition matrix is defined such that $\mathbf{d}$ and $\mathbf{u}$ are flux-normalized wavefields that have favourable reciprocity properties (Wapenaar 1998). Even though the inverse of $\mathbf{L}$ can be computed explicitly, this inverse becomes unstable because of a singularity at critical angles. To overcome this instability, we invert eq. (1) by means of a sparsity-promoting program that solves for the unknown downgoing and upgoing wavefields in the wavelet–curvelet domain. For this purpose, we define the sparsifying transform as $\mathbf{S} = \mathbf{C}_2 \otimes \mathbf{W}$, where $\mathbf{C}_2$ is the 2-D fast discrete curvelet transform (Candès *et al.* 2006a) along the source and receiver coordinates, $\mathbf{W}$ is the discrete wavelet transform (Mallat 2009), and the symbol $\otimes$ denotes the Kronecker product. Using this transform, we represent the one-way wavefield components as $\mathbf{d} = \mathbf{S}^*\mathbf{x}_d$ and $\mathbf{u} = \mathbf{S}^*\mathbf{x}_u$, where $\mathbf{x}_d$ and $\mathbf{x}_u$ are transform-domain coefficients and superscript * denotes the adjoint. We exploit the property of compressibility of wavefields in the curvelet domain (Candès *et al.* 2006b; Donoho 2006; Herrmann *et al.* 2008) by solving the following convex sparsity-promoting program

$$\underset{\mathbf{x}_d,\,\mathbf{x}_u}{\text{minimize}} \left\| \begin{bmatrix} \mathbf{x}_d \\ \mathbf{x}_u \end{bmatrix} \right\|_1 \text{ subject to } \left\| \begin{bmatrix} \mathbf{p} \\ \mathbf{v} \end{bmatrix} - \mathbf{L} \begin{bmatrix} \mathbf{S}^* & \mathbf{0} \\ \mathbf{0} & \mathbf{S}^* \end{bmatrix} \begin{bmatrix} \mathbf{x}_d \\ \mathbf{x}_u \end{bmatrix} \right\|_2 \leq \sigma,$$

where σ is a user-defined noise level that quantifies the tolerated mismatch in the forward problem. Subscripts 1 and 2 denote the ℓ_1- and ℓ_2-norm, respectively. We solve this problem with SPGℓ_1, a gradient-based method that uses spectral step-lengths and Pareto root-finding (Van den Berg & Friedlander 2008). Once estimates (denoted by the $\widehat{\ }$ symbol) for the coefficients $\widehat{\mathbf{x}}_d$ and $\widehat{\mathbf{x}}_u$ are found, we compute estimates for the downgoing field from $\widehat{\mathbf{d}} = \mathbf{S}^*\,\widehat{\mathbf{x}}_d$ and for the upgoing field from $\widehat{\mathbf{u}} = \mathbf{S}^*\,\widehat{\mathbf{x}}_u$.

We include a synthetic example derived from the Sigsbee model (Paffenholz *et al.* 2002) to demonstrate the performance of our algorithm on noisy data. Our findings are summarized in Fig. 1 for a case with 128 sources located at the surface and 128 receivers located below the salt. Gaussian noise is added to the data with SNR = 5.0 dB (signal-to-noise ratio, taken with respect to the total wavefield). Fig. 1(b) depicts a common-receiver gather of the pressure recordings. Together with the particle-velocity recordings, we use this recorded wavefield as input to our wavefield decomposition algorithm. We display estimates for common-receiver/source gathers of the upgoing component only, because they are weaker and therefore more challenging to recover. For reference, we also included in Fig. 1(c) a common-receiver gather obtained by explicitly inverting noise-free data. As expected, the common-receiver gather in Fig. 1(d) has a poor SNR ratio of SNR = 2.8 dB because it was obtained by direct inversion. The corresponding common-source gather in Fig. 1(e) is also of bad quality and contains, as we can see from the frequency–wavenumber plot, noise in the seismic frequency band and artefacts, denoted by the white arrows, which travel at the critical angle. When we compare these results with results obtained by sparsity promotion plotted in see Figs 1(g)–(i), we see significant improvements. We increased the SNR of Fig. 1(g) to SNR = 7.7 dB and we removed the instabilities at the critical angle (juxtapose Figs 1f and i). This results in a cleaner common-shot gather with preserved frequency content. In the next section, we use these improved estimates as input for our redatuming.

3 INTERFEROMETRIC REDATUMING

Given estimates for the decomposed wavefields, we are now in a position to create virtual data as if the sources and receivers are both located in the subsurface just above the target zone. Following earlier work by Wapenaar *et al.* (2008) and Herrmann & Wang (2008), we formulate interferometric redatuming as a wavefield inversion problem deriving from the following forward model in matrix–vector notation (Jumah & Herrmann 2011):

$$\mathbf{u} = \mathbf{D}\mathbf{g}, \tag{2}$$

where $\mathbf{u}$ is the estimated upgoing field (we dropped the hat for notational convenience), and $\mathbf{D}$ represents multidimensional convolution with the estimated downgoing wavefield. The action of this matrix involves forward Fourier transformation, followed by multidimensional convolution with the estimated time-harmonic downgoing wavefield, and inverse Fourier transformation. The vector $\mathbf{g}$ represents the unknown Green's function with virtual sources located at the receiver level for a medium that is homogeneous above the receivers.

It can easily be shown that interferometric redatuming by cross-correlation (Schuster & Zhou 2006; Bakulin & Calvert 2006) corresponds to applying the adjoint of $\mathbf{D}$ to the upgoing wavefield $\mathbf{u}$, yielding $\mathbf{c} = \mathbf{D}^*\mathbf{u}$. With eq. (2) this gives $\mathbf{c} = \mathbf{D}^*\mathbf{D}\mathbf{g}$. This expression is also known as the normal equation with $\mathbf{D}^*\mathbf{D}$ being the Hessian matrix whose columns contain point-spread functions (van der Neut 2012). In simple media and with ideal acquisition conditions (including flux-normalization at the source side), this Hessian approximates the identity so that $\mathbf{c}$ can be interpreted as a bandwidth- and dip-limited approximation of $\mathbf{g}$. However, this approximation is no longer valid in more complex geological settings that result in shadow zones, incomplete illumination, and multiple scattering. In this case, the action of the Hessian gives rise to location- and dip-dependent amplitude effects, spurious events, and a loss of frequency content. In this situation, eq. (2) should be inverted

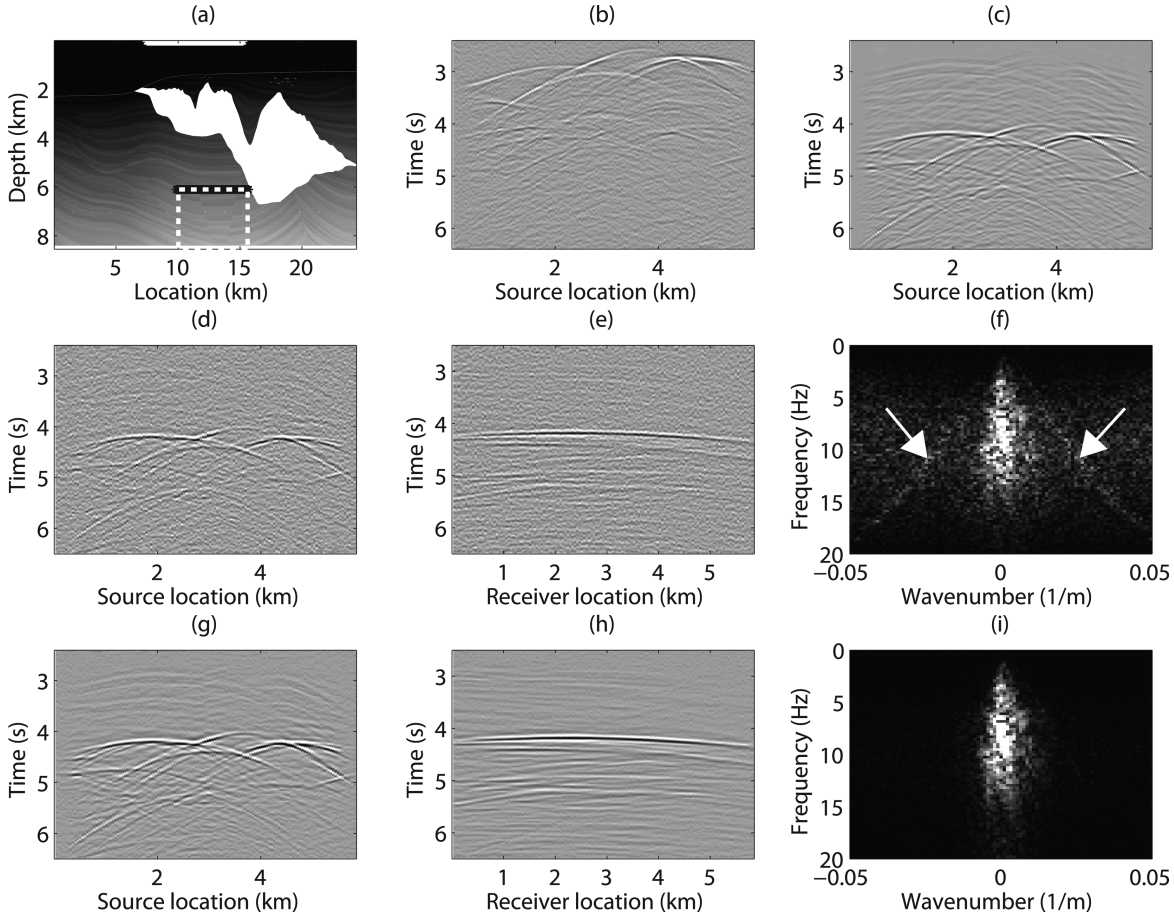

Figure 1. (a) Sigsbee model; the source and receivers arrays are given by the white solid line at the surface and by the black solid line in the subsurface (under the white dashed line), respectively. The white dashed line indicates the target area for imaging. (b) Common-receiver gather of the pressure field at receiver 65. Gaussian noise has been added. (c) Common-receiver gather of the upgoing field at receiver 65, retrieved with the algebraic inverse of **L**. No Gaussian noise has been added to the input data. (d) Same, from input data with Gaussian noise. (e) Common-source gather of the upgoing field at source 65, retrieved with the algebraic inverse of **L**. Gaussian noise has been added to the input data. (f) Same, in the frequency–wavenumber domain. (g) Common-receiver gather of the upgoing field at receiver 65, retrieved by sparse inversion. Gaussian noise has been added to the input data. (h) Common-source gather of the upgoing field at source 65, retrieved by sparse inversion. Gaussian noise has been added to the input data. (i) Same, in the frequency–wavenumber domain. Note that the signal has been preserved, whereas noise has been suppressed, especially near the critical angle.

properly to compensate for these effects to improve our estimate of **g**. A common approach to carry out inversion for ill-conditioned systems is to solve eq. (2) by regularized or damped least-squares inversion (Wapenaar *et al.* 2008). While computationally simple—that is, damped least squares has an analytic solution—this type of regularization leads to a loss in resolution and can still be numerically instable (van der Neut 2012). To overcome this difficulty, we follow Herrmann & Wang (2008) and use transform-domain sparsity as a prior to stabilize the inversion of eq. (2). As before, we represent the unknown wavefield—that is, the Green's function restricted to the source-receiver array at depth—in the wavelet–curvelet domain. Because wavefields compress in this domain, adding sparsity as a constraint helps to fill in the null space of **D** related to the finite bandwidth, the finite aperture, and the shadow zones caused by a complex overburden (e.g. by high-velocity salt bodies).

We illustrate interferometric redatuming by sparse inversion with the example introduced in Fig. 1. The results are summarized in Figs 2(a)–(c). For comparison, we include the output of interferometric redatuming by cross-correlation (Fig. 2a), where the source wavelet has been deconvolved from the retrieved responses for a fair comparison. We observe the strong reference reflector at approximately 1.5 s and the weaker reflections earlier in the gather. Aside from these clearly identifiable events, the estimated response contains artefacts and undesired amplitude effects, related to heterogeneities in the overburden, finite source aperture, multiple scattering and noise. Interferometric redatuming by damped least-squares inversion improves the results considerably (Fig. 2b), but the retrieved response is noisy, despite severe damping. The results of sparse inversion is relatively free of noise, while the temporal and spatial bandwidth of the signal has been well preserved, see Fig. 2(c). In the following section, the redatumed wavefields will be used for seismic imaging of the target zone below the well.

4 INTERFEROMETRIC IMAGING

The main purpose of the redatuming step is to create a virtual data set acquired just above the target zone. With these data we create an image of the target zone. Compared to conventional imaging, our approach has the advantage that no information on the background-velocity model of the medium above the receivers is needed. Since the computational domain of the target zone is relatively small, imaging will also be relatively cheap. To demonstrate this new imaging principle, we assume the background velocity to be known accurately within the target zone. In that case, linearization is

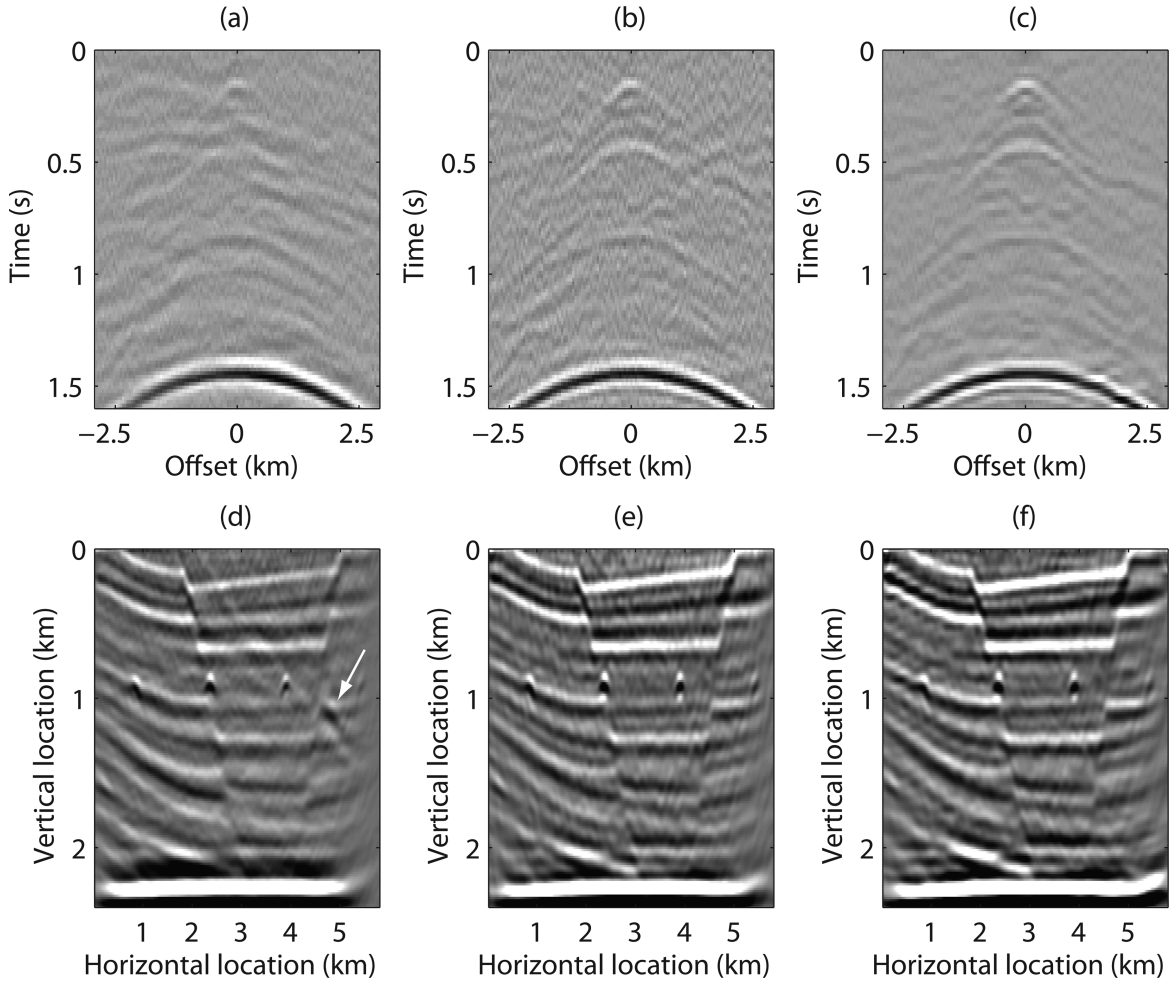

Figure 2. Virtual shot record as if there is a source at receiver 65, retrieved by (a) cross-correlation (the source wavelet has been deconvolved), (b) least-squares inversion and (c) sparse inversion. Migration results from virtual source data retrieved by (d) cross-correlation (the source wavelet has been deconvolved), (e) least-squares inversion and (f) sparse inversion.

accurate so that an image can be created by applying the adjoint of the single-scattering Born approximation to the redatumed data. Following Plessix & Mulder (2004), we write the linearized data, that is, the single scattering Green's function restricted to the array, as

$$\delta\mathbf{g} \approx \mathbf{K}\delta\mathbf{m}, \tag{3}$$

where the vector $\delta\mathbf{m}$ represents the perturbations with respect to the smooth background-velocity model in vectorized form and $\mathbf{K}$ is a matrix representing the discretized Born scattering operator. This matrix models wave propagation from the virtual sources to the perturbations within the target zone, followed by modelling of a single scattering and propagation back to the co-located receivers. Ignoring density variations, this imaging procedure corresponds to calculating $\delta\widehat{\mathbf{m}} = \mathbf{K}^*\mathbf{g}$. We implement this wave-equation based reverse-time migration procedure via the adjoint-state method for the time-harmonic Helmholtz equation (Plessix 2006). Because the background-velocity model below the receiver array is assumed to be known accurately, we apply the reverse-time migration operator directly to the redatumed data $\mathbf{g}$ from the example in the previous section.

The results of this procedure are summarized in Figs 2(d)–(f). Fig. 2(d) shows the results for Green's functions that are obtained by cross-correlation. The resolution is relatively poor due to the imprint of the point-spread function. We also observe an artefact identified by the white arrow. This artefact is likely caused by a reflection from the salt flank. As expected, the results obtained by inversion included in Figs 2(e)–(f) are artefact free. Although the image that was obtained after redatuming by sparse inversion (Fig. 2f) is less noisy than the image that was obtained after redatuming by least-squares inversion (Fig. 2e), these improvements are not very significant. This lack of improvement is not unexpected because the imaging procedure itself, consisting of applying the adjoint of $\mathbf{K}$ rather than the pseudo inverse, is now the limiting factor. We reason that in order to exploit the prospected advantages for interferometric imaging in an optimal way, sparsity should be promoted in the image space, rather than in the redatumed data space as we have done in this letter. To achieve this, interferometric redatuming can be applied in conjunction with sparsity-promoting least-squares migration, as we propose in the next section.

5 DISCUSSION

During sparsity-promoting least-squares migration, the forward model in eq. (3) is inverted using an iterative procedure that requires multiple evaluations of $\mathbf{K}$ and its adjoint $\mathbf{K}^*$ (Herrmann & Li 2012). While recent progress has been made to expedite this inversion by using techniques from compressive sensing, this type of imaging often remains prohibitively expensive because of the large

size of the model. Applying this method in conjunction with interferometric redatuming offers a cheaper alternative by conducting targeted imaging. This can be achieved by combining redatuming and imaging into a single step via substitution of eq. (3) into eq. (2) yielding $\mathbf{u} \approx \mathbf{DK}\delta\mathbf{m}$. The upgoing wavefield $\mathbf{u}$ is now related to the data-space operator $\mathbf{D}$, describing wave propagation (including internal multiples) above the receivers, and the model-space operator $\mathbf{K}$, describing wave propagation and reflections below the receivers. As before, we can invert this expression by solving a sparsity-promoting program in a suitable domain to estimate the velocity perturbations. As shown by Herrmann & Li (2012), curvelets play once more a pivotal role because they also sparsely represent velocity perturbations. Assuming that operator $\mathbf{D}$ can be computed for a particular depth level Λ in the subsurface (for instance, using the method of Wapenaar *et al.* (2012b)), this strategy can be used for imaging below Λ. Since operator $\mathbf{D}$ includes multiple scattering in the overburden (Wapenaar *et al.* 2008), all internal multiples above depth level Λ are mapped to the redatumed data, representing the response of the target zone. As shown by Tu *et al.* (2011) and Tu & Herrmann (2012), it is possible to replace the computationally expensive multidimensional convolution operation $\mathbf{DK}$ by a much cheaper to evaluate single Born scattering operator $\mathbf{K}$ that includes the downgoing field in the source function. Hence, interferometric imaging below Λ can be implemented with a computationally efficient single inversion step that combines interferometric redatuming to Λ and imaging below this level. This procedure can be further accelerated with techniques from compressive sensing, on which we plan to report elsewhere. Alternatively, eq. (2) can be inverted at level Λ and the retrieved Green's function $\mathbf{g}$, evaluated at zero time lag, can be interpreted as an (extended) non-linear image at this level (Vasconcelos *et al.* 2010).

6 CONCLUSION

Interferometric imaging consists of three steps, namely (i) decomposition of the recorded wavefields into downgoing and upgoing constituents, (ii) wavefield redatuming and (iii) imaging of the redatumed wavefields. Each step involves solving an inverse problem, which is ill-posed and therefore sensitive to noise. Solving these problems by damped least-squares inversion leads to a loss of resolution and can be numerically instable. Solving these problems with algorithms that promote sparsity in a transform-domain (such as curvelets) improves the resolution and reduces residual noise. To optimally appreciate these advantages in the final image, interferometric redatuming should be combined or integrated with least-squares migration. We have proposed a novel computationally efficient targeted seismic inversion methodology for this purpose that accounts for multiple scattering above a target horizon.

REFERENCES

Bakulin, A. & Calvert, R., 2006. The virtual source method: theory and case study, *Geophysics,* **71,** SI139–SI150.

Berkhout, A.J. & Verschuur, D.J., 2006. Focal transformation, an imaging concept for signal restoration and noise removal, *Geophysics,* **71,** A55–A59.

Broggini, F., Snieder, R. & Wapenaar, K., 2012. Focusing the wavefield inside an unknown 1D medium: beyond seismic interferometry, *Geophysics,* **77,** A25–A28.

Candès, E.J., Demanet, L., Donoho, D.L. & Ying, L., 2006a. Fast discrete curvelet transforms, *SIAM Multiscale Model. Simul.,* **5,** 861–899.

Candès, E.J., Romberg, J.K. & Tao, T., 2006b. Stable signal recovery from incomplete and inaccurate measurements, *Commun. Pure appl. Math.,* **59,** 1207–1223.

Claerbout, J.F., 1971. Toward a unified theory of reflector mapping, *Geophysics,* **36,** 467–481.

Donoho, D.L., 2006. Compressed sensing, *IEEE Trans. Informat. Theory,* **52,** 1289–1306.

Herrmann, F.J. & Hennenfent, G., 2008. Non-parametric seismic data recovery with curvelet frames, *Geophys. J. Int.,* **173,** 233–248.

Herrmann, F.J. & Li, X., 2012. Efficient least-squares migration with sparsity promotion and compressive sensing, *Geophys. Prospect.,* **60,** 696–712.

Herrmann, F.J. & Wang, D., 2008. Seismic wavefield inversion with curvelet-domain sparsity promotion, in *Proceedings of the 76th Annual Meeting, SEG, Expanded Abstracts,* Vol. 27, pp. 2497–2501, Las Vegas, USA.

Herrmann, F.J., Wang, D., Hennenfent, G. & Moghaddam, P.P., 2008. Curvelet-based seismic data processing: a multiscale and nonlinear approach, *Geophysics,* **73,** A1–A5.

Jumah, B. & Herrmann, F.J., 2011. Dimensionality-reduced estimation of primaries by sparse inversion, in *Proceedings of the 81th Annual Meeting, SEG, Expanded Abstracts,* pp. 3520–3525, San Antonio, TX, USA.

Lin, T.T.Y. & Herrmann, F.J., 2011. Robust source signature deconvolution and the estimation of primaries by sparse inversion, in *Proceedings of the 81th Annual Meeting, SEG, Expanded Abstracts,* pp. 4354–4358, San Antonio, TX, USA.

Mallat, S.G., 2009. *A Wavelet Tour of Signal Processing: The Sparse Way,* Academic Press, Burlington, MA, USA.

Mansour, H., Wason, H., Tim, T.T.Y. & Herrmann, F.J., 2012. Randomized marine acquisition with compressive sampling matrices, *Geophys. Prospect.,* **60,** 648–662.

Mehta, K., Kiyashchenko, D., Jorgensen, P., Lopez, J., Ferrandis, J. & Costello, M., 2010. Virtual source method applied to crosswell and horizontal well geometries, *Leading Edge,* **29,** 712–723.

Minato, S., Matsuoka, T., Tsuji, T., Draganov, D., Hunziker, J. & Wapenaar, K., 2011. Seismic interferometry using multidimensional deconvolution and crosscorrelation for crosswell seismic reflection data without borehole sources, *Geophysics,* **76,** SA19–SA34.

Paffenholz, J., McLain, B., Zaske, J. & Keliher, J., 2002. Subsalt multiple attenuation and imaging: observations from the sigsbee2b synthetic dataset, in *Proceedings of the 72nd Annual Meeting, SEG, Expanded Abstracts,* pp. 2122–2125, Salt Lake City, UT, USA.

Plessix, R.-E., 2006. A review of the adjoint-state method for computing the gradient of a functional with geophysical applications, *Geophys. J. Int.,* **167,** 495–503.

Plessix, R.E. & Mulder, W.A., 2004. Frequency-domain finite-difference amplitude-preserving migration, *Geophys. J. Int.,* **157,** 975–987.

Schuster, G.T. & Zhou, M., 2006. A theoretical overview of model-based and correlation-based redatuming methods, *Geophysics,* **71,** SI103–SI110.

Tu, N. & Herrmann, F.J., 2012. Imaging with multiples accelerated by message passing, in *Proceedings of the 82nd Annual Meeting, SEG, Expanded Abstracts,* Las Vegas, NV, USA.

Tu, N., Lin, T.T.Y. & Herrmann, F.J., 2011. Migration with surface-related multiples from incomplete seismic data, *Proceedings of the 79th Annual Meeting, SEG, Expanded Abstracts,* pp. 3222–3227, San Antonio, TX, USA.

Van den Berg, E. & Friedlander, M., 2008. Probing the pareto frontier for basis pursuit solutions, *SIAM J. Scient. Comput.,* **31,** 890–912.

van der Neut, J., 2012. Interferometric Redatuming by Multidimensional Deconvolution, *PhD thesis,* Delft University of Technology.

Vasconcelos, I., Sava, P. & Douma, H., 2010. Nonlinear extended images via image-domain interferometry, *Geophysics,* **75,** SA105–SA115.

Wapenaar, K., 1998. Reciprocity properties of one-way propagators, *Geophysics,* **63,** 1795–1798.

Wapenaar, K., Slob, E. & Snieder, R., 2008. Seismic and electromagnetic controlled-source interferometry in dissipative media, *Geophys. Prospect.,* **56,** 419–434.

Wapenaar, K., Broggini, F. & Snieder, R., 2012a. Creating a virtual source inside a medium from reflection data: heuristic derivation and stationary-phase analysis, *Geophys. J. Int.,* **190,** 1020–1024.

Wapenaar, K., Thorbecke, J., van der Neut, J., Slob, E., Broggini, F., Behura, J. & Snieder, R., 2012b. Integrated migration and internal multiple elimination, in *Proceedings of the 82nd Annual Meeting, SEG, Expanded Abstracts,* Las Vegas, NV, USA.